Bibliographical reference

Point Source Stimulated Acoustic Radiation of Cylindrical Shells: Resonance and Background Fields, Majid Rajabi and Mehdi Behzad, Acta Acustica **vol. 100** (Number 2), 2014, pp. 215-225

DOI
https://doi.org/10.3813/AAA.918701

ACTA ACUSTICA UNITED WITH ACUSTICA
Vol. 100 (2014) 215 – 225

DOI 10.3813/AAA.918701

Point Source Stimulated Acoustic Radiation of Cylindrical Shells: Resonance and Background Fields

Majid Rajabi, Mehdi Behzad
Department of Mechanical Engineering, Sharif University of Technology, Azadi Avenue, Tehran, Iran.
m_behzad@sharif.ir

Summary
Objective: The method of wave function expansion in association with the spatial Fourier transform technique is adopted to study the steady-state sound radiation characteristics of a cylindrical component of infinite length subjected to an arbitrary time-harmonic on-surface concentrated radial drive.
Method: Presenting the acoustical radiated coefficient as an exact function of modal accelerance function of the shell and following the classical Resonance Scattering Theory (RST), postulate that the radiated field can be synthesized as a superposition of the resonance response of the shell and a background signal within each partial wave. Utilizing the inherent background approach, we extracted the background (non-resonant) coefficients from the zero frequency limit of the three-dimensional (3-D) modal accelerance in the radiated coefficients for analogous liquid shells and the resonance components are isolated by the subtraction of these background coefficients from the radiated coefficients. Finally, the method of stationary phase is used to evaluate the formal integral expression for the total radiated pressure field and its resonant and background components in the frequency domain, for an observation point in the far-field.
Results: The far-field modal and total radiated acoustic pressure, background field and resonance spectra and their directivities are investigated for a water submerged aluminium cylindrical shell with different thicknesses and the usefulness of the proposed approach is discussed in details. The results exhibit the notable existence of non-resonant field for thin shells, where the resonances associated with Lamb and fluid-born A-type waves are expected to appear. The overall validity of results is established by comparison with the data in the existing literature.
PACS no. 43.20.-f, 43.20.El, 43.20.Fn, 43.20.Ks, 43.20.Mv, 43.20.Tb

1. Introduction

Cylindrical components (e.g., rods, tubes, pipes, pressure vessels, wires, fibers, shells, etc.) are frequently encountered in practical engineering. Consequently, there have been numerous studies on their dynamic behavior, and in particular, scattering and radiation of acoustic waves in such structures have been an active area of research for over a century. Here, the most important research works relevant to the present study shall be briefly reviewed.

Burroughs and Hallander [1] expressed analytical expressions for the far field acoustic radiation from an infinite fluid-loaded circular cylindrical shell reinforced with two sets of parallel periodic ribs. The cylindrical shell is excited by various types of concentrated mechanical point drives. Rebillard *et al.* [2], investigated the vibro-acoustic behavior of a finite cylindrical shell on which attached internal spring-mass systems and point defects are simulated in order to understand the radiation of machinery with a cylindrical hood. Ricks and Schmidt [3] illustrated a global matrix method for modeling layered cylindrical shells subjected to time-harmonic ring forces that can push on the shell in principal (i.e., radial, circumferential, and axial) directions. Guo [4] employed an asymptotic analysis to study the sound radiation from thin cylindrical shells driven by on-surface forces in terms of the shell- borne helical waves excited in the shell. It was found that the tangential forces acting on the shell drive more acoustic radiation than normal forces. Pathak and Stepanishen [5] used the classical integral transform technique in conjunction with the standard stationary phase method to address the problem of acoustic harmonic radiation from a fluid-loaded infinite cylindrical elastic shell subjected to arbitrary spatial loading. Constans *et al.* [6] utilized a material tailoring approach, based on finite element method (FEM) to present a numerical approach to minimize the radiated sound power from a vibrating shell structure driven with a point harmonic force input. Ko *et al.* [7] used the theory of elasticity to develop a theoretical model for evaluating the reduction of structure-borne noise generated by

Received 13 August 2013,
accepted 12 November 2013.

an axially symmetric ring force applied on the interior of a submerged coated cylindrical shell. Lecable *et al.* [8] employed the spatial Fourier transform along with the stationary phase method to develop a normal-mode series solution for acoustic radiation from a thick cylindrical elastic shell subjected to a point harmonic source. Skelton [9] investigated the time-harmonic line force excitation of an infinite elastic cylindrical shell immersed in compressible fluid and, in the asymptotic limit of heavy exterior fluid-loading. Li *et al.* [10] presented the parametric study on the far-field sound pressure radiated from an infinite fluid-filled/semi-submerged cylindrical shell excited by a radial point load. The influences of parameters such as fluid velocity, structural damping, position of the force, and structural thickness on the far-field sound pressure are investigated. Cuschieri [11] presented numerical results for the frequency dependant far-field acoustic radiation as a function of radiation angle for a fluid-loaded cylindrical shell with a compliant layer on its external surface, and excited by an internal radial ring force, using a normally reacting impedance layer model for the compliant layer. Yan *et al.* [12] developed an analytical method to investigate radiated sound power characteristics from an infinite submerged periodically stiffened cylindrical shell stimulated by a radial cosine harmonic line force. Following the statistical energy analysis (SEA), Ramachandran and Narayanan [13] presented a simplified analytical method to predict the modal density and the radiation efficiency of a longitudinally stiffened cylinder, by solving an eigenvalue problem based on strain energies and kinetic energies of the total structure. Tong *et al.* [14] proposed a direct boundary element method (BEM) and finite element method to study the acoustic radiation characteristics of a submerged structure. Model parameters of the structure and the fluid-structure interaction were analyzed by using FEM and direct BEM. Their simulations showed that their proposed direct-BEM/FEM method is more effective than FEM in computing the underwater sound radiation of the stern structure. More recently, Hasheminejad and Ahamdi-Savadkoohi [15], studied the vibro-acoustic behavior of a hollow functionally graded material (FGM) cylinder excited by on-surface mechanical drives. They examined the effects of FGM profile, cylinder thickness and excitation frequency on the radiated far-field acoustic pressure.

The RST postulates that each partial wave contained in the total scattering amplitude can be decomposed into two components: one is the background that is smooth and non-resonant, and the other represents a set of modal resonances of the scatterer [16, 17]. The resonances in the partial waves can be isolated by the subtraction of the background. Broad reviews of the sound scattering problems utilizing RST for resonance isolation purposes of cylindrical and spherical components can be found in the works of Gaunaurd [18], Uberall [19], Veksler [20], Hasheminejad and Rajabi [21] and Mitri [22].

Contrary to the notable research works on the acoustic resonance scattering problems, there is no strict study on the resonance isolation of acoustic radiated fields from cylindrical components under point source excitation (e.g., mechanical drives, laser). The main goal of this research is to cover this idea. Following the inherent background approach in RST, it is shown that there are two interacting components contributing to the modal accelerances [23, 24]. One is the non-resonant, which illustrates a regular behavior with respect to frequency and the other one is the resonant one illustrating singular behavior near the resonance frequencies. The resonant component influences the non-resonant component so that the magnitude of the accelerance changes quickly in the vicinity of the resonance frequencies, and slowly out of the resonance frequencies. Since the interaction between the resonant and non-resonant components occur in all frequency ranges, the non-resonant component hardly manifests its appearance in elastic shells. When the shear wave speed is set to be zero, like in the "liquid-shell background" by Veksler [25], the constant component can be observed. The coefficient of the constant component is extracted from the zero frequency limit of the modal accelerance of the analogous liquid shell due to the negligible interaction between the resonance and background signals near zero frequency. Making use of this approach, the expression of the modal background coefficients of the radiated field can be extracted from the zero frequency limits of the modal accelerances and the resonance coefficients are obtained by the subtraction of these background components from the total radiated pressure. Avoiding the near-field effects, the method of stationary phase is used to evaluate the formal integral expression obtained for the total radiated pressure and its components at an observation point in the far-field. Finally, to check the validity of the analysis, a numerical study is conducted for an aluminium shell with different thicknesses where various types of surface waves are expected to emerge in acoustic radiated field.

2. Formulation

2.1. Basic field equations

Consider the problem of sound radiation from an evacuated elastic hollow cylinder of infinite length, inner radius b and outer radius a, immersed in an acoustic medium of mean density ρ and sound speed c. The geometry of the problem is depicted in Figure 1. The body is subjected to a time-harmonic radial point source located at outer surface ($r = a$, $\theta = \theta_0$, $z = z_0$) which is modeled by

$$p_s(r = a, \theta, z, t) = aP_0\delta(\theta - \theta_0)\,\delta(z - z_0)\,\mathrm{e}^{-\mathrm{i}\omega t}, \tag{1}$$

where δ denotes the Dirac delta function, ω is the angular frequency and P_0 is a constant with the dimension of a pressure. The observation point is located at a distance R, a polar angle φ from the centerline of the shell (z-axis), and an azimuthal angle θ with respect to the x-axis. Following the linear acoustic regime, the pressure fluctuation in the surrounding acoustic medium, $p(r, \theta, z)$ is governed by the linear wave equation [26]

$$\nabla^2 p + k^2 p = 0, \tag{2}$$

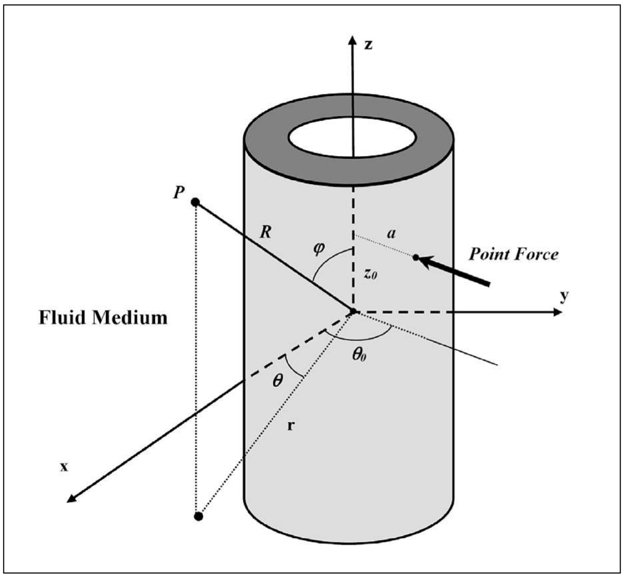

Figure 1. Problem Configuration.

in the domain defined by $r \geq a$, and $-\pi \leq \theta \leq \pi$, where $-\infty \leq z \leq \infty$, $k = \omega/c$ is the acoustic wave number, and the harmonic time dependence, $\exp(-\mathrm{i}\omega t)$, is suppressed here and henceforth. Also, the fluid displacement vector is written as [26]

$$U = \left(1/\rho\omega^2\right)\nabla p. \tag{3}$$

The displacement vector field of the isotropic homogeneous cylindrical shell can be expressed as sum of the gradient of a scalar potential ϕ and the curl of a vector potential $\boldsymbol{\psi} = (\psi_r, \psi_\theta, \psi_z)$ [8, 27],

$$\boldsymbol{u} = \nabla\phi + \nabla\times\boldsymbol{\psi}, \tag{4}$$

with the condition $\nabla\cdot\boldsymbol{\psi} = 0$. The above decomposition enables us to separate the dynamic equation of motion into the classical Helmholtz equations,

$$\left(\nabla^2 + k_p^2\right)\psi = 0, \tag{5a}$$

$$\left(\nabla^2 + k_s^2\right)\psi = 0, \tag{5b}$$

where $k_{p,s} = \omega/c_{p,s}$ are the elastic wave numbers, in which $c_p = \sqrt{(\lambda_s + 2\mu_s)/\rho_s}$ and $c_s = \sqrt{\mu_s/\rho_s}$ are the velocities of dilatational and distortional waves, respectively.

2.2. Resonance and background radiated coefficients

The solution of the problem may be obtained by the utilizing the spatial Fourier transform along the shell axis [28]

$$\tilde{f}(r,\theta,\xi,\omega) = \int_{-\infty}^{\infty} f(r,\theta,z,\omega)\mathrm{e}^{-\mathrm{i}\xi z}\,\mathrm{d}z, \tag{6a}$$

$$f(r,\theta,z,\omega) = \frac{1}{2\pi}\int_{-\infty}^{\infty} \tilde{f}(r,\theta,\xi,\omega)\mathrm{e}^{\mathrm{i}\xi z}\,\mathrm{d}\xi, \tag{6b}$$

where ξ is the Fourier transform parameter. After application of equation (6a) to the harmonic point source and the Helmholtz equation, the resulting partial differential equations can readily be solved by the standard method of variable separation. Accordingly, the transformed acoustic pressure may respectively be expanded as

$$\tilde{p}(r,\theta,\xi,\omega) = \sum_{n=0}^{+\infty} A_n(\xi,\omega)\,H_n^{(1)}(\eta r)\cos(n\theta), \tag{7}$$

where $H_n^{(1)}$ is the Hankel function of the first kind, $\eta = \sqrt{k^2-\xi^2}$ and A_n denotes the acoustical radiated coefficients to be determined by the appropriate boundary conditions (Appendix), and are given by

$$A_n = -\frac{\tilde{p}_{s,n}F_n(\omega)}{H_n^{(1)'}(x) - H_n^{(1)}(x)F_n(\omega)}, \tag{8}$$

where prime denotes differentiation with respect to the argument, $x = \eta a$. $\tilde{p}_s(\theta,\xi,\omega)$ denotes the Fourier transform of the point force which can be expressed as

$$\tilde{p}_s(\theta,\xi,\omega) = \sum_{n=0}^{+\infty} \tilde{p}_{s,n}\cos(n\theta),$$

where

$$\tilde{p}_{s,n}(\theta,\xi,\omega) = \frac{aP_0}{2\pi}\,\varepsilon_n\cos(n\theta_0)\,\mathrm{e}^{-\mathrm{i}\xi z_0}$$

and symbol ε_n is the Neumann factor ($\varepsilon_n = 1$ for $n = 0$, and $\varepsilon_n = 2$ for $n > 0$) In addition, $F_n(\omega) = Z_n^{2,1}/Z_n^{1,1}$, where $Z_n^{1,1}$ and $Z_n^{2,1}$ are the 6×6 minor determinants of the first two elements in the first column of a 7×7 matrix, $\boldsymbol{Z}_n$, whose elements are given by Veksler [20]. The function $F_n(\omega)$ is called the modal accelerance function of the shell in literature [23, 24], which depends on the characteristics of the bulk waves in the shell implicitly. (The proper expansions associated to the potential functions equation (5) are given in Appendix).

Making a suitable analogy between the inherent background approach developed for scattering phenomena and the present stimulated radiation event, the background radiation coefficient is obtained by substituting the zero frequency limits of the modal accelerance functions in the radiation coefficient for analogous liquid shell as

$$A_n^b = -\frac{\tilde{p}_{s,n}F_n(0^+)}{H_n^{(1)'}(x) - H_n^{(1)}(x)F_n(0^+)}, \tag{9}$$

where $F_n(0^+)$ can be analytically derived by using the following approximations for cylindrical functions for $x \ll 1$,

$$J_n(x) = \frac{x^n}{2^n n!}, \tag{10a}$$

$$Y_n(x) = \frac{2}{\pi}\ln x \quad \text{for} \quad n = 0, \tag{10b}$$

$$Y_n(x) = -\frac{(n-1)!}{\pi}\left(\frac{2}{x}\right)^n \quad \text{for} \quad n \geq 1, \tag{10c}$$

in the relation of modal accelerance function $F_n(\omega) = Z_n^{2,1}/Z_n^{1,1}$, which leads to

$$F_n(0^+) = -\frac{\rho_s}{\rho}\frac{1}{\ln(b/a)} \quad \text{for} \quad n = 0, \tag{11a}$$

$$F_n(0^+) = -\frac{\rho_s}{\rho}n\frac{1+(b/a)^{2n}}{1-(b/a)^{2n}} \quad \text{for} \quad n \geq 1. \tag{11b}$$

It is noticeable that in the above formulations, it is assumed that the Fourier transform of the radiated acoustic pressure in the fluid, satisfies the classical Sommerfeld radiation condition [29].

2.3. Total and modal resonance and background components of radiated pressure and far-field approximation

Finally, by applying the inverse Fourier transform, equation (6b), to equation (7), the radiated acoustic pressure may be written as

$$p(r,\theta,z,\omega) = \frac{1}{2\pi}\int_{-\infty}^{+\infty}\tilde{p}(r,\theta,\xi,\omega)\mathrm{e}^{\mathrm{i}\xi z}\,\mathrm{d}\xi \tag{12}$$
$$= \frac{1}{2\pi}\int_{-\infty}^{+\infty}\sum_{n=0}^{+\infty}A_n(\xi,\omega)\,H_n^{(1)}(\eta r)\cos(n\theta)\mathrm{e}^{\mathrm{i}\xi z}\,\mathrm{d}\xi.$$

In the near field, analytic evaluation of the above integral is very complicated. However, in the far-field, it can always be approximated by the method of stationary phase which proposes $\xi = k\cos\varphi$ as the point of stationary phase [8]. Following the standard method, the far-field approximation of integral (12) with respect to the stationary phase is obtained as

$$p(R,\theta,z,\omega) = \sum_{n=0}^{+\infty}p_n \tag{13}$$
$$= \frac{1}{\pi\sqrt{k\sin\varphi}}\left[\sum_{n=0}^{+\infty}i^{-(n+1)}A_n(k\cos\varphi,\omega)\cos(n\theta)\right]\frac{\mathrm{e}^{\mathrm{i}kR}}{R}.$$

The background component of the above pressure can be written as

$$p^{(b)}(R,\theta,z,\omega) = \sum_{n=0}^{+\infty}p_n^{(b)} \tag{14}$$
$$= \frac{1}{\pi\sqrt{k\sin\varphi}}\left[\sum_{n=0}^{+\infty}i^{-(n+1)}A_n^{(b)}(k\cos\varphi,\omega)\cos(n\theta)\right]\frac{\mathrm{e}^{\mathrm{i}kR}}{R},$$

and similarly, the resonant component is

$$p^{(res)}(R,\theta,z,\omega) = \sum_{n=0}^{+\infty}p_n^{(res)} \tag{15}$$
$$= \frac{1}{\pi\sqrt{k\sin\varphi}}$$
$$\cdot\left[\sum_{n=0}^{+\infty}i^{-(n+1)}A_n^{(res)}(k\cos\varphi,\omega)\cos(n\theta)\right]\frac{\mathrm{e}^{\mathrm{i}kR}}{R},$$

where the modal resonance amplitude, $A_n^{(res)}$, is evaluated by subtracting the modal background amplitude from the modal radiated coefficient as

$$A_n^{(res)} = A_n - A_n^{(b)}. \tag{16}$$

In equations (13) to (15), p_n, $p_n^{(b)}$, $p_n^{(res)}$ denote the modal radiated pressure, modal background and modal resonance. This completes the necessary background required for the analysis of the problem.

3. Numerical Results

In this section, we consider some numerical examples in order to demonstrate effectiveness of proposed approach. Considering the large number of parameters involved here while keeping in view our computing hardware limitations, we confine the calculations to some particular model. The aluminium shell is assumed to be evacuated and surrounded by water ($\rho = 1000\,\mathrm{kg/m^3}$, $c = 1480\,\mathrm{m/s}$) at atmospheric pressure and ambient temperature. The mechanical properties of the aluminium shell is specified as $\rho_s = 2790\,\mathrm{kg/m^3}$, $\lambda_s = 61.15\,\mathrm{GPa}$, $\mu_s = 24.85\,\mathrm{GPa}$.

A MATLAB® code was constructed for computing equations (8)–(9), calculating the unknown radiation, background and resonance radiation coefficients as a function of the nondimensional frequency ka. The computations were performed on a Pentium IV personal computer with a frequency resolution $\Delta ka = 0.01$, polar angle resolution of $\Delta\varphi = 0.001$ rad and maximum truncation constant of $n_{\max} = ka + 30$ especially selected to assure convergence in the case of a thick shell and also in the high frequency range. The convergence was systematically checked in a simple trial and error manner, by increasing the truncation constant, n, (i.e., by including more modes in all summations) while looking for stability in the numerical value of the solutions. Also, the far-field value of the radial coordinate for calculating the far-field radiated pressure amplitude was chosen $R = 10a$ so that fair convergence of the results achieved.

Before presenting the main numerical results, we shall establish the overall validity of the calculations. Accordingly, we first computed the normalized far-field pressure amplitude, $|p(R = 10a,\theta,z,\omega)/P_0|$, versus dimensionless frequency, ka, and axial parameter, z/a, for a radially-driven ($\theta = \theta_0 = \pi$, $z_0 = 0$), water-submerged homogeneous steel shell, by setting $h/a = 0.2$, $\rho_s = 7800\,\mathrm{kg/m^3}$, $\lambda_s = 113\,\mathrm{GPa}$, $\mu_s = 75.9\,\mathrm{GPa}$ in our general MATLAB code. The outcome as shown in Figure 2 exhibits an excellent agreement with that displayed in Figure 4 of [8].

In the first step, our aim is to study the behavior of the proposed background (non-resonant) component of radiated pressure. Figure 3 shows the variations of the normalized background component, $|p^{(b)}/P_0|$ at the observation point ($R = 10a$, $\theta = \theta_0$, $z = z_0 = 0$), in a selected frequency range (i.e. $0 < ka < 50$), for selected thickness parameters of the shell ($h/a = 0.01$, 0.04, 0.1, 0.5,

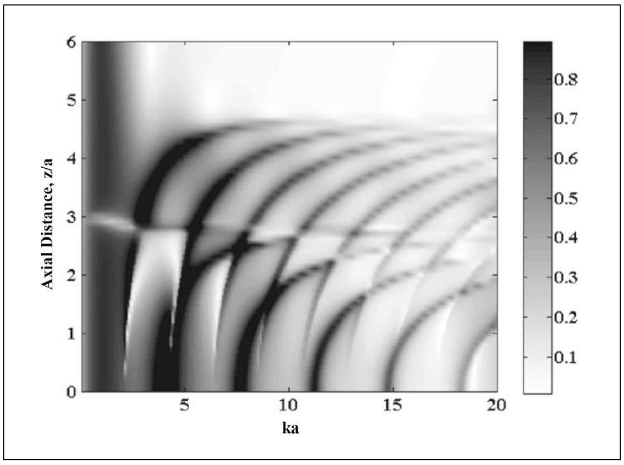

Figure 2. The top view of the variation of the normalized far-field pressure amplitude, $|p(R = 10a, \theta, z, \omega)/P_0|$ versus dimensionless frequency and axial parameter for a radially-driven ($\theta = \theta_0 = \pi$, $z = z_0 = 0$) water-submerged homogeneous steel shell.

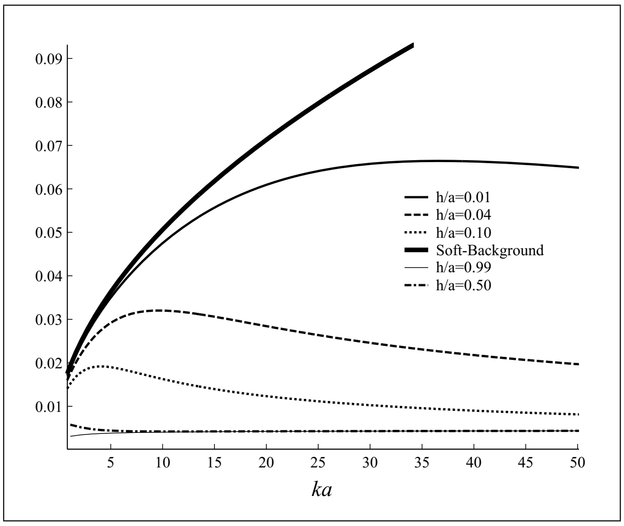

Figure 3. The variations of the normalized background component, $|p^{(b)}/P_0|$ at the observation point ($R = 10a$, $\theta = \theta_0$, $z = z_0 = 0$), versus dimensionless frequency, for selected thickness parameters of the aluminium shell ($h/a = 0.01$, 0.04, 0.1, 0.5, 0.99)) and soft-background.

0.99). For comparison, the soft-background which represents the normalized acoustic radiation corresponding to a cylindrical cavity with the same geometry is also plotted by setting the accelerance coefficients $F_n(\omega) \to \infty$. As this figure shows, the background component depicts a smoothly increasing trend with frequency up to a certain frequency and then a smoothly decreasing trend, for all thickness values. The frequency of this switching is increased (decreased) as the shell wall thickness decreases (increases), where for the soft-background, which resembles a zero thickness shell (i.e. $h/a \to 0$), tends toward infinity. For very thick hollow cylinder, this frequency tends to zero so that this switching is not occurred. For very low frequencies, $ka \ll F_n(0^+)$, especially as the shell thickness decreases, the trend approaches the soft-background.

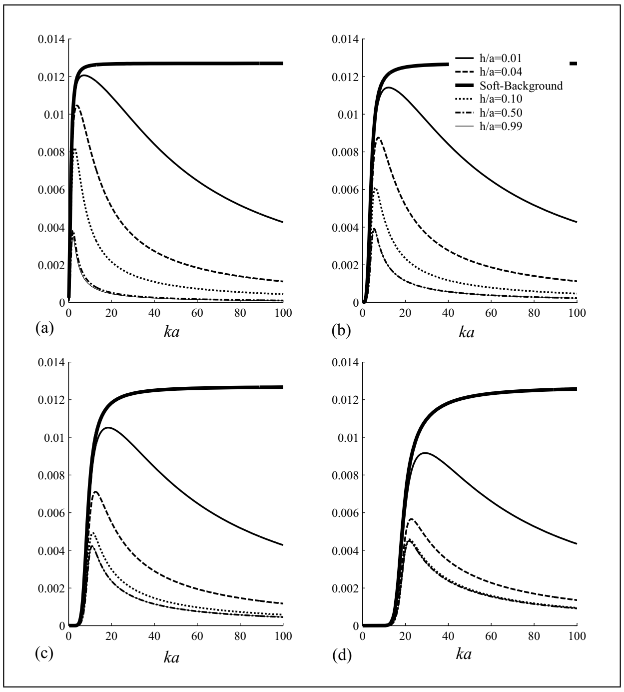

Figure 4. The variations of the normalized modal components of background radiation, $|p^{(b)}/P_0|$, for $h/a = 0.04$ aluminium shell, for selected mode numbers (a) $n = 2$, (b) $n = 5$, (c) $n = 10$, (d) $n = 20$.

This behavior bear a resemblance to the behavior of the background component of scattering fields in scattering problems [23, 24]. For better examination of the proposed background approach, we studied the modal components of the background radiation for selected mode numbers (a) $n = 2$, (b) $n = 5$, (c) $n = 10$, (d) $n = 20$, in Figure 4. As these plot show, the general trend is the same for different thicknesses and mode numbers; increasing to a specific frequency and then slightly decreasing. Considering equation (9), it could be shown that this transition frequency is characterized by $ka^* = F_n(0^+)$. As the mode number or shell wall-thickness are increased, the transition frequency increases. For the soft-background case, the curves tend to right and approach a constant value. In general, as the shell thickness is decreased, the background amplitude increases and approaches the soft-background, especially at frequencies below the transition frequency, however, the differences are increased at higher frequencies. Also, for thick shells (where their behavior approaches to those of rigid bodies), the amplitude of background component decreases for all frequency ranges. It makes this perception that the influence of background field on the total radiated field is insignificant for thick shells. Focusing on the low frequency ranges, as the mode number is increased, a rest frequency domain is appeared in which no background component exists. This observation promises a completely resonant radiation of the shell in this domain. It may be predicted that the influence of background component on the total radiated pressure spectrum is much more pronounced for frequency ranges between the maximum frequency of rest domain and the frequencies of the same order of the transition frequency.

Here, we intend to examine the accuracy of the proposed theory of background component (hidden within the radiation field), and evaluate the usefulness of the approach for resonance isolation, especially for thin shells where the contribution of background signal is pronounced. Figure 5 shows the variation of normalized far-field radiated pressure, $|p/P_0|$, and its background, $|p^{(b)}/P_0|$, and resonance components, $|p^{(res)}/P_0|$, at the observation point $R = 10a$, $\theta = \theta_0$, $z = z_0 = 0$), in a selected frequency range (i.e. $0 < ka < 40$), for a thin aluminum shell (i.e. $h/a = 0.04$). As this figure shows, the radiated pressure consists of a resonance spectrum superimposed on the proposed smooth background component. The resonance modes in the spectrum are linked to the standing surface waves which are formed around the cylindrical shell. Making comparison with the information of resonance scattering spectrum of a $h/a = 0.04$ thickness aluminium shell provided by Veksler [20], the resonances are simply identified as zero-order symmetric Lamb and fluid-borne A type waves. The symbols "S_0", and "A" designate the resonances associated with the n'th vibration mode of zero-order symmetric Lamb waves and fluid born A-type waves, respectively. As it is seen, the resonances corresponding to fluid-borne A-type waves, especially those who appear as peaks in pressure spectrum, demonstrate noticeable amplitudes where the resonances of Lamb waves depict as dips in the spectrum. The appearance of resonances as peaks or dips are generally linked to this fact that as the shell is stimulated, the surface waves are generated and propagated on the shell surface. These waves decay gradually and re-radiate the acoustic waves in the surrounding fluid medium. Hence, when these surface waves and their associate radiated acoustic waves are out of phase (in phase), the resonances appears as dips (peaks) in the spectrum.

For better assessment of our proposed hypothesis of existence of a non-resonant constituent in the point source stimulated radiated field, we focus on the modal response of the shell. Figure 6 shows the variation of normalized modal radiated pressure amplitude, $|p/P_0|$, modal background amplitude, $|p^{(b)}/P_0|$, and modal resonance amplitude, $|p^{(res)}/P_0|$, of the shell for selected mode numbers (a) $n = 0$, (b) $n = 1$, (c) $n = 2$, (d) $n = 3$, (e) $n = 4$, (f) $n = 22$, (g) $n = 23$, (h) $n = 23$, (i) $n = 25$, (j) $n = 26$. For $n = 0$ case (monopole mode), a notably high peak is observed at a very low frequency, which is called the "giant monopole" resonance (i.e., analogous situation of air bubbles in water) [30]. This resonance is not projected in the total radiated pressure, but is clear in the resonant component. For mode numbers $n = 1, \ldots, 4$, where the resonances corresponding to the zero-order Lamb wave are excited, the modal radiated pressure perfectly coincides with the background component, except in the resonance region where the resonances are very clearly isolated. For these modes of vibration, the response of the shell is accompanied with the background (non-resonant) radiation field where the proposed background clearly predicts its contribution. For high mode numbers $n = 22, \ldots, 26$, where

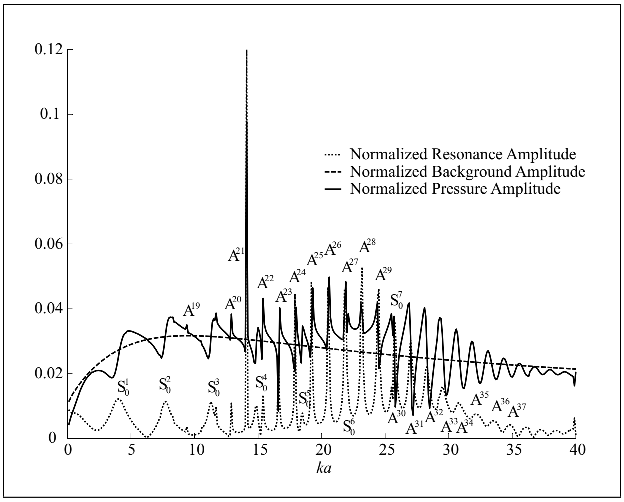

Figure 5. The variation of normalized far-field radiated pressure, $|p/P_0|$, and its background, $|p^{(b)}/P_0|$, and resonance components, $|p^{(res)}/P_0|$, at the observation point ($R = 10a$, $\theta = \theta_0$, $z = z_0 = 0$), versus dimensionless frequency, for $h/a = 0.04$ aluminum shell.

the resonances corresponding to fluid-borne A-type waves are anticipated to be excited, the modal radiated pressure is approximately in resonant modes; because the background component in the selected frequency range is in its rest regime, especially for cases (g)–(j). In these cases, the background effect is negligible and the shell behaves as a pure resonator. For resonances located in these frequency ranges, the radiation spectrum at the resonant frequencies emerges as a peak.

Figure 7 illustrates the angular distribution of the far-field total normalized pressure amplitude, $|p(\omega, \theta)/P_0|$, normalized background amplitude, $|p^{(b)}(\omega, \theta)/P_0|$, and normalized resonance amplitude, $|p^{(res)}(\omega, \theta)/P_0|$, at selected wave numbers $ka = 11.12$, 14.84, 15.25 corresponding to the resonance frequencies S_0^3, S_0^4 and A^{22}, observed in Figure 6, respectively. The point force direction (i.e. $\theta_0 = 0$, $z_0 = 0$) is shown by an arrow. As these figures exhibit, the number of main lobes seen in the resonance scattering directivity plots are exactly twice the mode number corresponding to each resonance frequency, or in other word, twice the number of wavelengths corresponding to each standing wave which fit the perimeter of the guiding circle in the shell [20]. It is notable that this equality is not necessarily true for the angular diagrams of the total radiated pressure amplitude.This is due to the interactions of the resonance component of the radiated waves with the background component within the total radiated pressure. Nevertheless, the resonance radiation directivities exhibit a more uniform pattern than those associated with the radiated pressure, especially at frequencies stretched out in the transition frequency (i.e. ka^*) domain, which relieve the resonance classification process. The results clearly display the essence and effectiveness of the presented approach based on the subtraction of the background component from the corresponding far-field radiated pressure amplitude in order to isolate and identify the resonance frequencies.

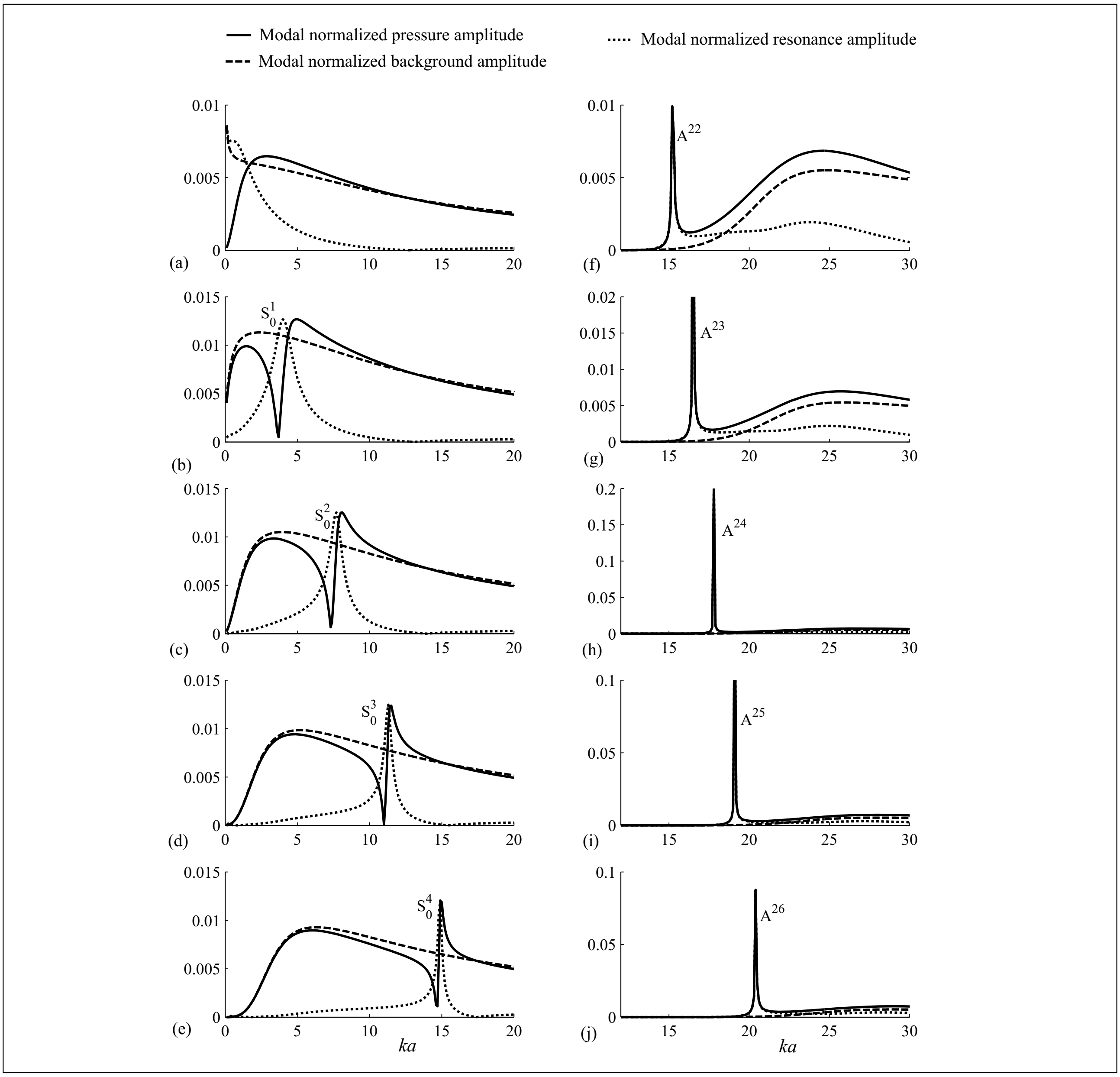

Figure 6. The variation of normalized modal radiated pressure amplitude, $|p_n/P_0|$, modal background amplitude, $|p^{(b)}/P_0|$, and modal resonance amplitude, $|p^{(res)}/P_0|$, of $h/a = 0.04$ aluminum shell and for selected mode numbers (a) $n = 0$, (b) $n = 1$, (c) $n = 2$, (d) $n = 3$, (e) $n = 4$, (f) $n = 22$, (g) $n = 23$, (h) $n = 24$, (i) $n = 25$, (j) $n = 26$.

As it was established before [31, 32], the excited resonance characteristics (i.e., frequency and bandwidth) of the surface waves are polar angle dependant. Considering the analogy between the oblique incident scattering problems and the point source radiation problems, the general information of shell resonances, as a result of phase matching phenomenon of circumferential and guided leaky waves, is the same for both cases. Considering the appearance of the so-called guided waves and the variation of wave propagation style associated to surface waves from circumferential type to helically mode, for out of (x, y)-plane observation points (i.e., non-zero incident angle for scattering problems), the examination of polar angle dependency for the point source stimulated radiation problem may be helpful essentially due to its inherent value as a canonical problem in physical acoustics. Also, potential applications include material characterization and nondestructive testing/evaluation of materials especially for those whose axial characters are the goal. Furthermore, considering the recent decade research works in acoustic radiation [8] and acoustic scattering problems [31, 32], dealing with the helically surface waves and leaky guided waves, establish the complexity and importance of the subject. Lecable *et al.* [8] evaluated the acoustic pressure radiated from cylindrical shells subjected to a point force using the stationary phase method and the fast Fourier transform (FFT) technique. In their results, the emergence of an infinite number of spatial dis-

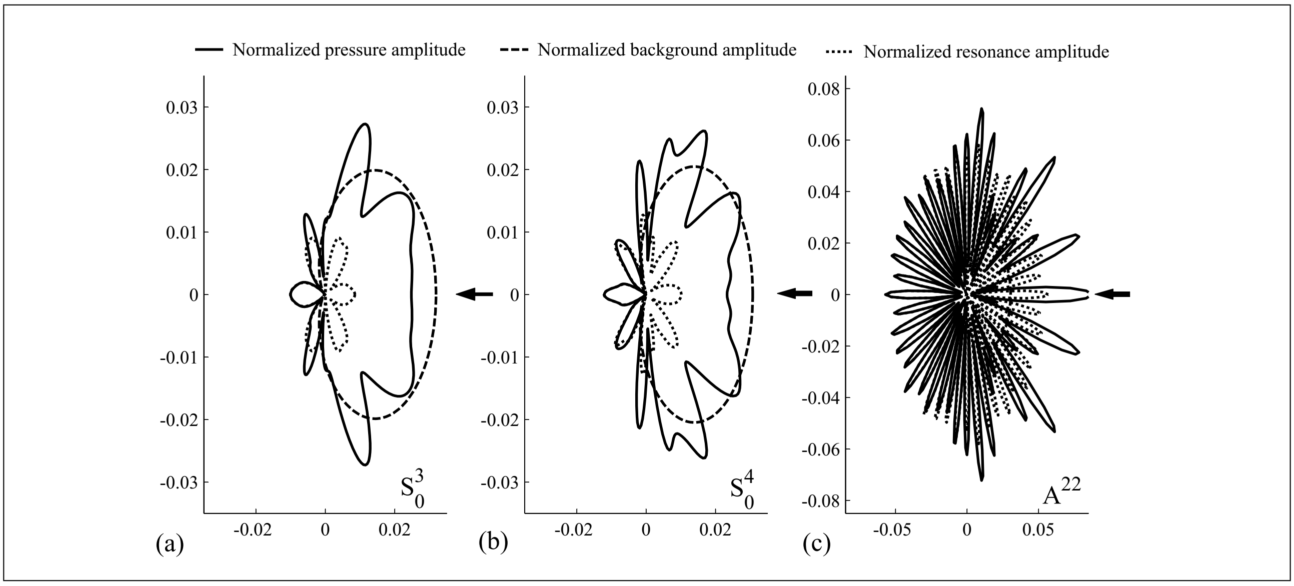

Figure 7. The angular distribution of the far-field total normalized pressure amplitude, $|p(\omega,\theta)/P_0|$, normalized background amplitude, $|p^{(b)}(\omega,\theta)/P_0|$, and normalized resonance amplitude, $|p^{(res)}(\omega,\theta)/P_0|$, at selected wave numbers (a) $ka = 11.12$, (b) $ka = 14.84$, (c) $ka = 15.25$, for $h/a = 0.04$ aluminum shell.

persion curves associated to each leaky wave propagating on the cylindrical body, calculated via FFT technique was reported and compared with the single dispersion curve obtained by the stationary phase method. Fan *et al.* [33] analyzed the oblique scattering problem from cylindrical bodies. They reported and explained outstanding features including the pairing of one axially guided mode with each transverse whispering gallery mode, the appearance of an anomalous pseudo-Rayleigh in the cylinder at incidence angles greater than the Rayleigh angle, and distortional effects of the longitudinal whispering gallery modes on the entire resonance spectrum of the cylinder. Also, Mitri [34] showed that for an aluminium cylinder, there exist acoustic backscattering enhancements at low dimensionless frequencies, $ka \ll 0.1$. Honaravr *et al.* [35] made an effort to provide physical explanation for the mentioned observation by Mitri [34], by establishing a correlation between helical surface waves and the longitudinal and flexural guided modes propagating inside a cylindrical body.

In order to consider the subject, the proposed definition of the resonant component of radiated pressure, equation (15), is used, which reflects both the center frequency and bandwidth (i.e., all information contained in the complex frequency) of each resonance mode. Here, we just focus on the modal response of the shell to avoid the busy and complication of the total response of the body. The third and twenty second modes, $n = 3$ and $n = 22$, are selected among the first analyzed thirty vibration modes in which the resonances associated to symmetric/asymmetric Lamb waves and fluid-borne A type wave are expected to be excited, respectively, for the previously mentioned $h/a_{q+1} = 0.04$ thickness aluminium shell.

Figures 8 and 9 are the top views of normalized far-field total pressure amplitude, $|p(\omega,\varphi,\theta = 0)/P_0|$, and its resonance component, $|p^{(res)}(\omega,\varphi,\theta = 0)/P_0|$, respectively,

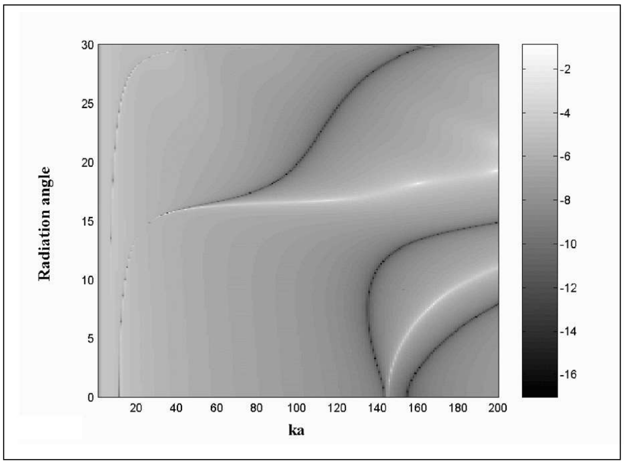

Figure 8. The top view of the variation of normalized far-field modal pressure amplitude, $|p_n(\omega,\varphi,\theta = 0)/P_0|$, for $n = 3$ for $h/a = 0.04$ aluminum shell.

corresponding to $n = 3$ plotted as a function of polar angle for the selected frequency range (i.e. $0 < ka < 200$). To improve the plots, the amplitudes are modified using logarithm function (i.e. $\log_e$). In order to relieve the comparison between the results with the dispersion curves extracted from resonance scattering problems [20], the complementary angle of polar angle, (i.e. radiation angle: $\varphi' = \pi/2 - \varphi$), is used as the vertical axis variable. As these figures show, the resonances corresponding to the symmetric/asymmetric Lamb and Guided waves emerge as bright lines in the plots, where their thickness indicate the bandwidth of the resonances. The symbols S_i^n, A_i^n and G^n designate the resonances corresponding to the i'th order symmetric/asymmetric Lamb waves and guided waves, respectively.

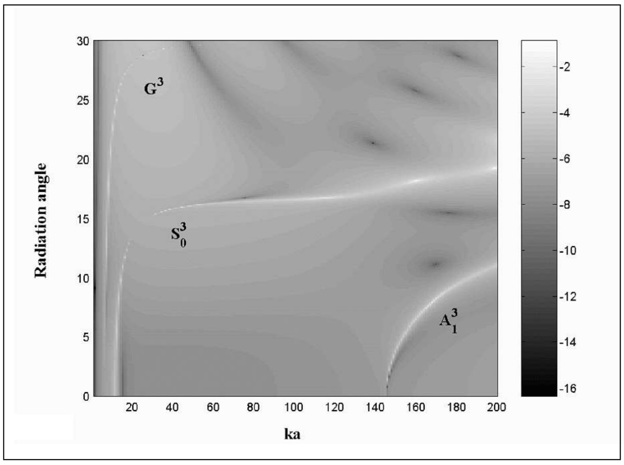

Figure 9. The top view of variation of normalized far-field modal resonance pressure amplitude, $|p^{(res)}(\omega, \theta)/P_0|$, for $n = 3$ of an $h/a = 0.04$ aluminum shell.

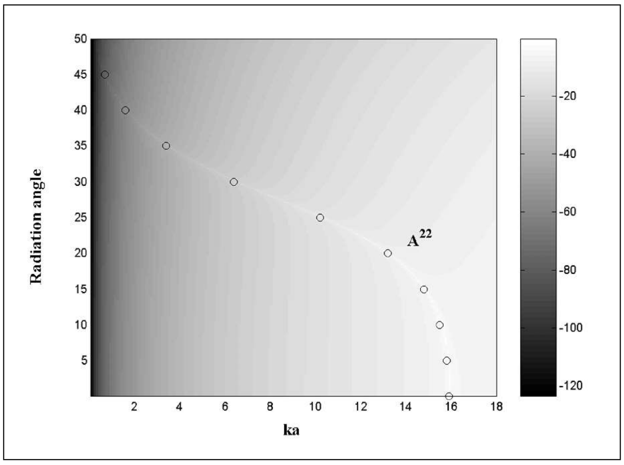

Figure 10. The top view of the variation of normalized far-field modal resonance pressure amplitude, $|p^{(res)}(\omega, \theta)/P_0|$, for $n = 22$ of an $h/a = 0.04$ aluminum shell.

As it is observed, the resonance frequencies generally increase with the increase of φ'. This right-ward shift is in agreement with the observation made by Conoir *et al.* [31, 32]. Considering the analytical expression of resonance frequencies associated to n'th partial mode, $f_{res} = nc_{ph}/(2\pi a \cos\gamma)$ (in which c_{ph} denotes the phase velocity of the wave and γ indicates the helix angle of helically wave propagation direction with respect to cross-section of body, this phenomenon is interpreted in this way that the higher radiation angles corresponds to the higher helix angles in general and therefore higher values of γ leads to an increase in associated resonance frequency, f_{res} [31, 32]. Also, as it is expected, by increasing (decreasing) the φ' (i.e. radiation angle), the zero order Lamb wave approaches the true Rayleigh wave (on a submerged plate), and the corresponding resonance frequencies approach the Rayleigh angles, $\varphi'_R \simeq 32°$. Also, the higher order symmetric/asymmetric Lamb and guided waves approach the shear waves, and the corresponding resonance frequencies tend to shear critical angle, $\varphi_c^{'s} \simeq 28.4°$. This conversion occurs at frequencies too higher than our selected frequency range [20, 36]. The most important observations in these figures is the appearance of fake anti-resonance branches (i.e. dark curves) in Figure 8 as the results of interference of background and resonance components in each resonance mode. As it is clear, the subtraction of the proposed background signals will remove these fake resonance curves.

Figure 10 depicts the polar angle dependency of resonances associated to the fluid-borne A-type wave corresponding to the mode number $n = 22$, the same as Figure 9. Due to its low amplitude, it is rather difficult to follow the excited resonance. Therefore, the trend of the resonance is marked by the circle symbol. This type of resonance occurs at lower frequencies for higher radiation angle. This is in contrary to other surface waves; i.e., symmetric/asymmetric Lamb and Guided waves in our examples, and also Rayleigh and Whispering Gallery waves in cylinders [36]. This phenomenon is interpreted considering that the phase velocity of surface waves depends on the polar angle, (i.e. $c_{ph} = c/\sqrt{\sin^2\varphi' + (n/ka^{(res)})^2}$) so that an increase in φ' leads to a decrease in c_{ph}. Mathematically, if the rate of decrease in c_{ph} is sufficiently greater than the rate of decrease of $\cos\gamma$ in the formula $f_{res} = nc_{ph}/(2\pi a \cos\gamma)$, the resonance frequencies occur at lower frequencies.

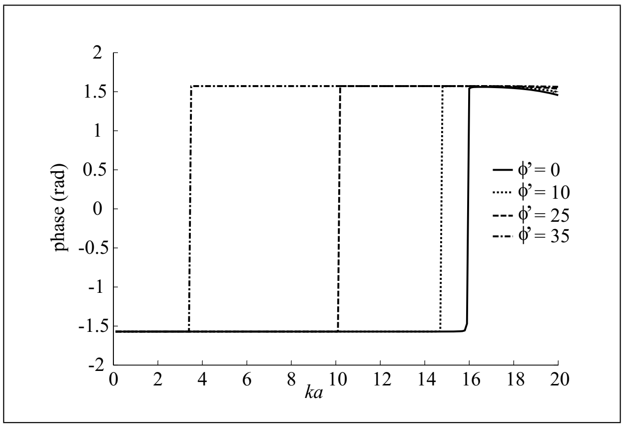

Figure 11. The phase variation of resonant pressure modulus as a function of frequency and for selected radiation angles (i.e., φ' = 0°, 10°, 25°, 35°).

In addition to the above mentioned happening, a further singular feature is also seen where the fluid-borne A-type wave is still alive at radiation angles greater than longitudinal critical angle, $\varphi_c^{'p} \simeq 13.6°$ and shear critical angle, $\varphi_c^{'s} \simeq 28.4°$. To assure that the curve has a resonant nature, the phase of the resonant component is computed as a function of frequency and for selected radiation angles (i.e. $\varphi' = 0°, 10°, 25°, 35°$) exhibited in Figure 11. As seen in this figure, all phase curves show a sudden π rad phase shift at corresponding resonance frequencies. This feature is physically explained by the origin of this type of fluid-borne waves. This type of wave is the interaction between the zero-order asymmetric Lamb wave and the Franz-type, and does not possess any cut-off frequency, as same as the zero-order symmetric and asymmetric Lamb waves. As the radiation angle approaches the shear critical angle (i.e. $\varphi_c^{\prime s} \simeq 28.4°$), the contribution of asymmetric Lamb wave dies away, and the wave nature become the Franz type, which merely depends on the obstacle geometry and is directly related to the external creeping waves in the surrounding fluid medium.

4. Conclusions

Presenting the acoustical radiated coefficients as an exact function of modal accelerance function of the shell using the spatial Fourier transform technique, and making a proper analogy with the scattering problems and also exploiting the inherent background approach in acoustic resonance scattering regime, we extracted the radiated background (non-resonant) coefficients from the zero frequency limit of the modal accelerance in the radiated coefficients for analogous liquid shells and the resonance components are isolated by the subtraction of these background coefficients from the radiated coefficients. The results exhibit that the acoustic resonance characteristics of the elastic homogeneous shells can effectively be analyzed by taking advantage of the proposed background approach. The proposed theory may be helpful essentially due to its inherent value as a canonical subject in physical acoustics. Also, potential applications include material characterization, nondestructive testing/evaluation of materials and noise control engineering etc.

Appendix

A1. The Fourier expansion of potential functions

$$\tilde{\phi}(r,\theta,\xi,\omega) = \frac{1}{\rho_s\omega^2}\sum_{n=0}^{+\infty}\big(B_n(\xi,\omega)\,\Upsilon_n(\eta_p r) + C_n(\xi,\omega)\,\Pi_n(\eta_p r)\big)\cos(n\theta), \quad \text{(A1a)}$$

$$\tilde{\psi}_r(r,\theta,\xi,\omega) = \frac{1}{\rho_s\omega^2}\sum_{n=0}^{+\infty}\big(D_n(\xi,\omega)\,\Upsilon_{n+1}(\eta_s r) + E_n(\xi,\omega)\,\Pi_{n+1}(\eta_s r)\big)\sin(n\theta), \quad \text{(A1b)}$$

$$\tilde{\psi}_\theta(r,\theta,\xi,\omega) = -\frac{1}{\rho_s\omega^2}\sum_{n=0}^{+\infty}\big(D_n(\xi,\omega)\,\Upsilon_{n+1}(\eta_s r) + E_n(\xi,\omega)\,\Pi_{n+1}(\eta_s r)\big)\cos(n\theta), \quad \text{(A1c)}$$

$$\tilde{\psi}_z(r,\theta,\xi,\omega) = \frac{1}{\rho_s\omega^2}\sum_{n=0}^{+\infty}\big(F_n(\xi,\omega)\,\Upsilon_n(\eta_s r) + G_n(\xi,\omega)\,\Pi_n(\eta_s r)\big)\sin(n\theta). \quad \text{(A1d)}$$

B_n through G_n are unknown Fourier coefficients. Depending on the polar angle, φ, and the longitudinal and transverse critical angles, $\varphi_c^{p,s}$, where $\varphi_c^{p,s} = \cos^{-1}(c/c_{p,s})$, the characteristic functions (Υ_n and Π_n) are the first and second kind cylindrical Bessel functions (J_n and Y_n) or the first and second kind of the modified Bessel functions (I_n and K_n) according to Table A1 (see [37]).

Table A1. Characteristic functions of wave propagation in elastic body.

	$\varphi_c^p < \varphi$	$\varphi_c^s < \varphi < \varphi_c^p$	$\varphi < \varphi_c^s$
η_p	$\sqrt{k_p^2 - \xi^2}$	$\sqrt{\xi^2 - k_s^2}$	$\sqrt{\xi^2 - k_s^2}$
η_s	$\sqrt{k_s^2 - \xi^2}$	$\sqrt{k_s^2 - \xi^2}$	$\sqrt{\xi^2 - k_s^2}$
$\Upsilon_n(\eta_p r)$	$J_n(\eta_p r)$	$I_n(\eta_p r)$	$I_n(\eta_p r)$
$\Pi_n(\eta_p r)$	$Y_n(\eta_p r)$	$K_n(\eta_p r)$	$K_n(\eta_p r)$
$\Upsilon_n(\eta_s r)$	$J_n(\eta_s r)$	$J_n(\eta_p r)$	$I_n(\eta_s r)$
$\Pi_n(\eta_s r)$	$Y_n(\eta_s r)$	$Y_n(\eta_s r)$	$K_n(\eta_s r)$

A2. Boundary Conditions

The appropriate boundary conditions imposed at the inner ($r = b$) and the outer ($r = a$) surfaces of the shell are given here where the relation between pertinent stress components and the displacement vector is given in [27].

A2.1. Boundary conditions at outer surface ($r = a$)

These conditions are explicitly written as the equilibrium of the radial stress with the applied external radial load and fluid pressure at the outer surface ($r = a$),

$$\tilde{\sigma}_{rr}(r=a,\theta,\xi,\omega) = -\tilde{p}_s(\theta,\xi,\omega) - \tilde{p}(r=a,\theta,\xi,\omega). \quad \text{(A2)}$$

Vanishing of the shear stresses at the outer surface ($r = a$) gives

$$\tilde{\sigma}_{r\theta}(r=a,\theta,\xi,\omega) = \tilde{\sigma}_{rz}(r=a,\theta,\xi,\omega) = 0. \quad \text{(A3)}$$

Also, the continuity of the normal fluid and solid displacements at the outer surface ($r = a$) leads to

$$\tilde{u}_r(r=a,\theta,\xi,\omega) = \tilde{U}_r(r=a,\theta,\xi,\omega). \quad \text{(A4)}$$

A2.2. Boundary conditions at inner surface ($r = b$)

At the inner surface of the body, ($r = b$), vanishing of the radial and tangential stresses gives

$$\tilde{\sigma}_{rr}(r=b,\theta,\xi,\omega) = \tilde{\sigma}_{r\theta}(r=b,\theta,\xi,\omega) = \tilde{\sigma}_{rz}(r=b,\theta,\xi,\omega) = 0. \quad \text{(A5)}$$

References

[1] C. B. Burroughs, J. E. Hallander: Acoustic radiation from fluid-loaded, ribbed cylindrical shells excited by different types of concentrated mechanical drives. J. Acoust. Soc. Am. **91** (1992) 2721–2739.

[2] E. Rebillard, B. Laulagnet, J. L. Guyader: Influence of an embarked spring-mass system and defects on the acoustical radiation of a cylindrical shell. App. Acoust. **36** (1992) 87–106.

[3] D. C. Ricks, H. Schmidt: A numerically stable global matrix method for cylindrically layered shells excited by ring forces. J. Acoust. Soc. Am. **95** (1994) 3339–3349.

[4] Y. P. Guo: Radiation from cylindrical shells driven by on-surface forces. J. Acoust. Soc. Am. **95** (1994) 2014–2021.

[5] A. G. Pathak, P. R. Stepanishen: Acoustic harmonic radiation from fluid-loaded infinite cylindrical elastic shells using elasticity theory. J. Acoust. Soc. Am. **96** (1994) 573–582.

[6] E. W. Constans, G. H. Koopmann, A. D. Belegundu: The use of modal tailoring to minimize the radiated sound power of vibrating shells: theory and experiment. J. Sound. Vib. **217** (1998) 335–350.

[7] S. H. Ko, W. Seong, S. Pyo: Structure-borne noise reduction for an infinite elastic cylindrical shell. J. Acoust. Soc. Am. **109** (2001) 1483–1495.

[8] C. Lecable, J. M. Conoir, O. Lenoir: Acoustic radiation of cylindrical elastic shells subjected to a point source: investigation in terms of helical acoustic rays. J. Acoust. Soc. Am. **110** (2001) 1783–1791.

[9] E. A. Skelton: Line force receptance of an elastic cylindrical shell with heavy exterior fluid loading. J. Sound. Vib. **256** (2002) 131–153.

[10] H. L. Li, C. J. Wu, X. Q. Huang: Parametric study on sound radiation from an infinite fluid-filled / semi-submerged cylindrical shell. App. Acoust. **64** (2003) 495–509.

[11] J. M. Cuschieri: The modeling of the radiation and response Green's function of a fluid-loaded cylindrical shell with an external compliant layer. J. Acoust. Soc. Am. **119** (2006) 2150–2169.

[12] J. Yan, T. Y. Li, T. G. Liu: Characteristics of the vibrational power flow propagation in a submerged periodic ring-stiffened cylindrical shell. App. Acoust. **67** (2006) 550–569.

[13] P. Ramachandran, S. Narayanan: Evaluation of modal density, radiation efficiency and acoustic response of longitudinally stiffened cylindrical shell. J. Sound. Vib. **304** (2007) 154–174.

[14] Z. Tong, Y. Zhang, Z. Zhang, H. Hua: Dynamic behavior and sound transmission analysis of a fluid–structure coupled system using the direct-BEM/FEM. J. Sound. Vib. **299** (2007) 645–655.

[15] S. M. Hasheminejad, A. A. Savadkoohi: Vibro-acoustic behavior of a hollow FGM cylinder excited by on-surface mechanical drives. Composite Struct. **92** (2010) 86–96.

[16] L. Flax, L. R. Dragonette, H. Uberall: Theory of elastic resonance excitation by sound scattering. J. Acoust. Soc. Am. **63** (1978) 723–731.

[17] L. Flax, G. C. Gaunaurd, H. Uberall: Theory of resonance scattering. Physical Acoustics XV., Academic, New York, 1980, 191–294.

[18] G. C. Gaunaurd: Elastic and acoustic resonance wave scattering. App. Mech. Rev. **42** (1989) 143–192.

[19] H. Uberall: Acoustic resonance scattering. Gordon and Breach Science, Philadelphia, 1992.

[20] N. D. Veksler: Resonance acoustic spectroscopy. Springer Series on Wave Phenomena, Springer-Verlag, Berlin, 1993.

[21] S. M. Hasheminejad, M. Rajabi: Acoustic resonance scattering from a submerged functionally graded cylindrical shell. J. Sound. Vib. **302** (2007) 208–228.

[22] F. G. Mitri: Generalized theory of resonance excitation by sound scattering from an elastic spherical shell in a nonviscous fluid. IEEE Transactions on Ultrasonicsm Ferroelectric. Freq. Cont. **59** (2012) 1781–1790.

[23] M. S. Choi, Y. S. Joo: Theory of the background amplitudes in acoustic resonance scattering. J. Acoust. Soc. Am. **101** (1997) 2083–2087.

[24] M. S. Choi, Y. S. Joo, J. P. Lee: Inherent background coefficients for submerged cylindrical shells. J. Acoust. Soc. Am. **101** (1997) 1743–1745.

[25] N. D. Veksler: Intermediate background in problems of sound waves scattering by elastic shells. Acustica **76** (1992) 1–9.

[26] A. D. Pierce: Acoustics, an introduction to its physical principles and applications. American Institute of Physics, New York, 1991.

[27] J. D. Achenbach: Wave propagation in elastic solids. North-Holland, New York, 1976.

[28] F. B. Hilderbrand: Methods of applied mathematics. Prentice Hall of India, 1961.

[29] M. C. Junger, D. Feit: Sound, structures and their interaction. 2nd ed. MIT Press, Cambridge, MA, 1986.

[30] J. D. Murphy, E. D. Breitenbach, H. Uberall: Resonance scattering of acoustic waves from cylindrical shells. J. Acoust. Soc. Am. **64** (1978) 677–683.

[31] J. M. Conoir, J. L. Izbicki, P. Rembert: Scattering by cylindrical objects at oblique incidence. – In: Acoustic Interaction With Submerged Elastic Structures. Series on Stability, Vibration and Control of Systems, Series B, Vol. 5. Scientific, Singapore, 1996.

[32] J. M. Conoir, P. Rembert, O. Lenoir, J. L. Izbicki: Relation between helical surface waves and elastic cylinder resonances. Resonances shift and guided waves polarization study. J. Acoust. Soc. Am. **93** (1993) 1300–1307.

[33] Y. Fan, F. Honarvar, A. N. Sinclair, M. R. Jafari: Circumferential resonance modes of solid elastic cylinders excited by obliquely incident acoustic waves. J. Acoust. Soc. Am. **113** (2003) 102–113.

[34] F. G. Mitri: Acoustic backscattering enhancements resulting from the interaction of an obliquely incident plane wave with an infinite cylinder. Ultrasonics **50** (2010) 675–682.

[35] F. Honarvar, E. Enjilela, A. N. Sinclair: Correlation between helical surface waves and guided modes of an infinite immersed elastic cylinder. Ultrasonics **51** (2011) 238–244.

[36] J. David, N. Cheeke: Fundamental and application of ultrasonic waves. CRC Series in Pure and Applied Physics, 2002.

[37] F. Leon, F. Lecroq, D. Decultot, G. Maze: Scattering of an obliquely incident acoustic wave by an infinite hollow cylindrical shell. J. Acoust. Soc. Am. **91** (1992) 1388–1397.